ISSN 1330-3651(Print), ISSN 1848-6339 (Online)
Received: 20 August 2025; Accepted: 27 December 2025

https://doi.org/10.17559/TV-20250820002917
Original scientific paper

Robust and High-Precision Harmonic Estimation of Shaking Table Vibrations Using Accelerometer and Cheetah Optimization

Kadir Yasin SUNCA*, Serdar KOÇKANAT

Abstract: The accuracy of shaking tables in seismic simulations is limited by harmonic distortions in acceleration signals resulting from the inherent nonlinearity of the system. This study presents a novel approach based on the Cheetah Optimization (CO) algorithm for estimating the amplitude and phase components of these harmonics. The algorithm's performance was first validated against other metaheuristic methods in the literature on a standard test signal and was found to be successful. Subsequently, the CO algorithm was applied to data obtained from a real-time shaking table experimental setup. These experiments included testing the system under loaded and unloaded conditions, at three different displacement levels (3.55 mm, 5 mm, 10 mm) and with three different waveforms: sinusoidal, triangular, and square. The results showed that the CO algorithm exhibited very high estimation accuracy for sinusoidal signals in both load cases. However, the algorithm's performance degraded under load on triangular signals and struggled to accurately model the signal in all scenarios due to the sharp transitions and high harmonic content of square waveforms. These findings suggest that while CO has proven to be an effective method for shaking table vibration analysis, particularly for sinusoidal signals, additional model improvements are necessary for more complex waveforms.

Keywords: acceleration harmonic identification; nonlinear output regulation; optimization algorithms; vibration control

1 INTRODUCTION

Earthquakes are seismic events caused by the sudden release of energy accumulated in the Earth's crust. While thousands of small earthquakes occur daily worldwide, several hundred medium- to large-scale earthquakes are recorded annually. Earthquakes are especially devastating in densely populated cities with poor building infrastructure, leading to building collapses, infrastructure damage, and loss of life [1].

Shaking tables are essential tools for studying the behaviour of buildings and structural elements by simulating earthquake effects in a controlled and repeatable manner. By applying either real earthquake recordings or artificially generated seismic waves to a structure, these devices enable engineers to observe material deformations, assess structural strength, and identify potential damage mechanisms. This information helps engineers improve design standards, detect vulnerabilities in existing buildings, and design structures that are safer and more resilient to future earthquakes. In summary, shake tables provide the scientific foundation for earthquake safety [2]. Shaking tables are experimental systems where displacement, velocity and acceleration parameters are controlled, consisting of mechanical, electrical or hydraulic systems [3].

Estimating acceleration harmonics in shaking tables is crucial for improving the system's dynamic accuracy and control stability. In electro-hydraulic shaking systems, inherent nonlinearities - such as friction, dead zones, and backlash in components like actuators and servo valves - cause harmonic distortions in the acceleration response. These harmonic components, which appear as integer multiples of the fundamental frequency, result in deviations from the target acceleration signal and impede the accurate reproduction of earthquake motions on the test structure. Acceleration harmonic estimation facilitates the identification of these distortions in terms of frequency and amplitude, enabling the effective implementation of adaptive compensation, filtering, or feed-forward control strategies. Consequently, this process enhances the system's bandwidth, reduces dynamic response errors, and significantly improves the repeatability and fidelity of earthquake simulations [4].

Recently, various techniques have been developed to estimate acceleration harmonics in shaking table systems. The Fast Fourier Transform (FFT) is the most commonly used fundamental method for this purpose. By converting the acceleration signal from the time domain to the frequency domain, the FFT enables harmonic estimation. However, due to limitations such as estimation challenges and spectral overlap, researchers have increasingly turned to optimization methods, which have proven effective for harmonic estimation. Harmonic estimation has been addressed not only through classical optimization techniques such as NLMS and RLS but also by employing artificial neural network and Kalman filter methods, which aim to overcome the limitations of conventional approaches [5]. In shaking table systems, harmonic estimation of acceleration signals is particularly challenging in nonlinear hydraulic systems, and classical methods often prove limited. Consequently, metaheuristic algorithms have been increasingly employed in recent years. Yao et al. proposed using the Simulated Annealing algorithm to accurately estimate acceleration harmonics in hydraulic servo shaking tables. Their approach demonstrated high precision and improved real-time performance compared to the Recursive Least Squares (RLS) method, all without requiring prior knowledge of the system [6]. Similarly, Yao et al. analyzed the harmonic estimation performance of Particle Swarm Optimization (PSO) and the Water Cycle Algorithm, evaluating the convergence and predictive capabilities of these algorithms [7, 8]. In a subsequent study, Kockanat combined a Modified Artificial Bee Colony (MABC) algorithm with RLS to simultaneously estimate and eliminate harmonics [9]. Although this approach is effective in both estimation and harmonic reduction, the complexity and computational cost of the algorithm are disadvantages. Malathy et al. developed a hybrid heuristic algorithm for harmonic estimation and elimination [10]. Although the method offers flexibility and comprehensive performance, the hybrid structure's complexity and long computation time are notable disadvantages.

In this study, a real-time experimental shaking table system was developed, and the resulting acceleration signals were measured and recorded using advanced Sensebox7001 accelerometers. To estimate the harmonics, present in these acceleration signals, the CO Algorithm was implemented. This algorithm has demonstrated higher accuracy than many well-known metaheuristic and hybrid algorithms in solving large-scale benchmark problems such as CEC2010 and CEC2013. Furthermore, to comprehensively evaluate harmonic estimation performance, the shaking table was operated under both loaded and unloaded conditions. For each scenario, acceleration harmonic signals with sinusoidal, square, and triangular waveforms were generated, and their amplitudes were varied to perform an extensive parameter sweep. This approach provides a broader and more diverse signal set than most existing studies in the literature. Analysis of the collected data demonstrated the effectiveness of the CO-based harmonic estimation method.

2 EQUIPMENTS USED IN EXPERIMENTAL SETUP

The experimental setup consisted of a shaking table, an accelerometer, and a computer equipped with software capable of controlling the shaking table and recording accelerometer data. The 50 × 50 cm single-axis shaking table can simulate dynamic motions in up to three dimensions and operate both with and without load [11]. Fig. 1 illustrates the shaking table under unloaded and loaded conditions. The shaking table features a travel distance of ±80 mm, a frequency range of up to 30 Hz, 16-bit control precision, a load capacity of 1000 N, and operates at 220 V. Driven by a servo motor with closed-loop PID and TVC control, the system supports both predefined and user-defined waveforms.

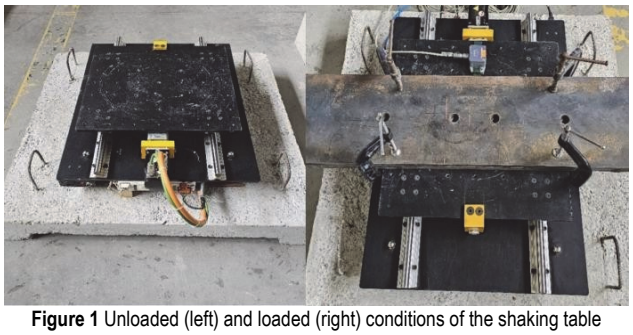

Figure 1 Unloaded (left) and loaded (right) conditions of the shaking table

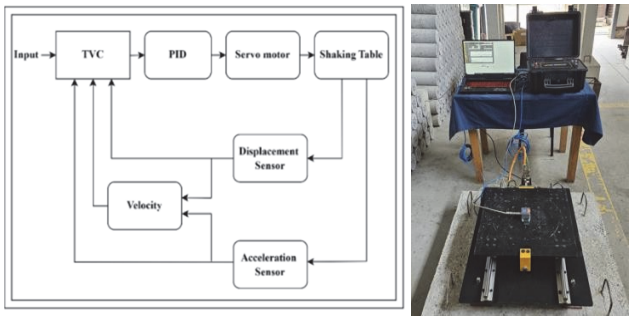

Figure 2 Control scheme (left) and experimental setup (right) of the shaking table

The control scheme of the shaking table and the overall experimental setup are shown in Fig. 2. The employed accelerometer is the Sensebox7001, a low-noise MEMS device that offers high sensitivity, stability, and low power consumption. It measures acceleration by detecting changes in velocity and transmitting this data to a processing unit. Fig. 3 illustrates its connection to the shaking table.

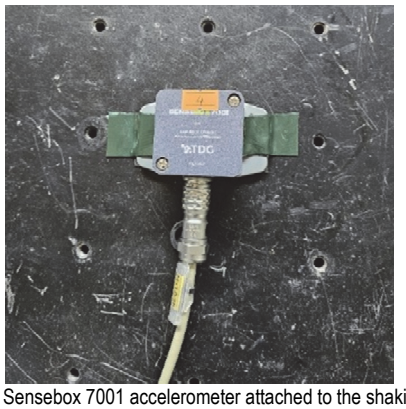

Figure 3 Sensebox 7001 accelerometer attached to the shaking table

In this study, predefined sinusoidal, square, and triangular waveforms with varying acceleration amplitudes were applied to both loaded and unloaded shaking table systems under computer control. For each configuration, the system output was recorded using high-precision Sensebox7001 accelerometers, and harmonic acceleration signals were obtained. These recorded signals were then analysed for the harmonic estimation problem using the proposed CO based estimation approach.

3 CHEETAH OPTIMIZATION ALGORITHM

Cheetah optimization (CO) algorithm is a next-generation heuristic optimization algorithm inspired by the lives of cheetahs in nature and first introduced by Akbari et al. in 2022 [12]. It is particularly notable for its ability to produce highly accurate solutions to continuous and complex optimization problems.

CO algorithm involves four main phases: search, sit and wait, attack, and retreat and relax. These phases are illustrated in Fig. 4.

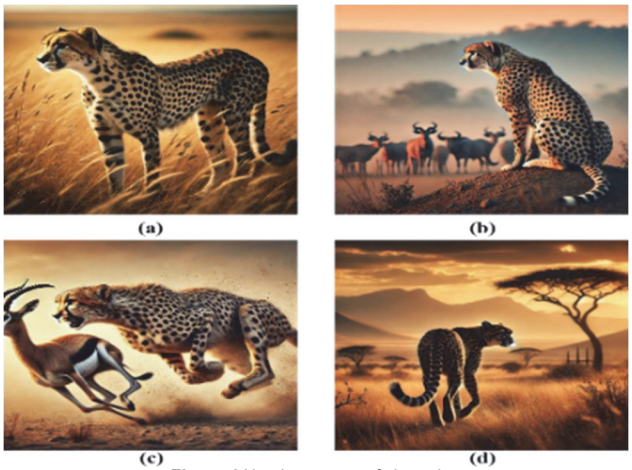

Figure 4 Hunting stages of cheetahs.

The search behavior is mathematically expressed as:

$$X_{i,j}^{t+1} = X_{i,j}^{t} + r_{i,j}^{-1} \cdot a_{i,j}^{t} \quad (1)$$

where $X_{i,j}^{t+1}$ and $X_{i,j}^{t}$ denote the current and updated positions of cheetah i in dimension j. $r_{i,j}^{-1}$ is a randomization parameter and $a_{i,j}^{t}$ is the step length at iteration t. The step length is generally defined as $a_{i,j}^{t} = 0.001 \times t / T$, where T is the maximum iteration count. In the sit and wait phase, the cheetah remains stationary to avoid alerting the prey, modelled as:

$$X_{i,j}^{t+1} = X_{i,j}^{t} \tag{2}$$

This mechanism prevents premature convergence by maintaining population diversity. Once the prey is within range, the attack phase begins, where cheetahs adjust their positions rapidly toward the prey's location:

$$X_{i,j}^{t+1} = X_{B,j}^{t} + r_{i,j} \cdot \beta_{i,j}^{t} \tag{3}$$

where $X_{B,j}^{t}$ is the current position of the prey in plane j. $r_{i,j}$ and $\beta_{i,j}^{t}$ are the turning factor and interaction factor of cheetah i in plane j, respectively. These adaptive strategies collectively enable the CO algorithm to balance exploration and exploitation efficiently.

CO algorithm offers several advantages, including a simple structure, fast convergence, and a robust balance between exploration and exploitation due to its adaptive, hunting-inspired phases. Its dynamic position update mechanism enables it to efficiently avoid local minima and achieve high solution accuracy in complex optimization problems. However, the CO algorithm also has some limitations, such as sensitivity to parameter tuning and a potential risk of premature convergence in high-dimensional search spaces or when population diversity decreases over iterations.

4 MATHEMATICAL MODELLING

The sinusoidal harmonic signal $h(t)$ in acceleration harmonic estimation problems is composed of a sum of harmonics with uncertain phase and amplitude values. It is expressed as follows:

$$h(t) = \sum_{n=1}^{Q} A_n \sin\left(2\pi n f_0 t + \varphi_n\right) \tag{4}$$

Here, f_0 is the fundamental frequency, A_n is the amplitude, φ_n is the phase, and Q is the number of harmonics. A_0 represents the direct current (DC) component, and $n(t)$ is the noise added to the random harmonic signal [6, 9, 10]. Thus, the newly modelled $h(t)$ is expressed as follows:

$$h(t) = \sum_{n=1}^{Q} A_n \sin\left(2\pi n f_0 t + \varphi_n\right) + A_0 + n(t) \tag{5}$$

The harmonic signal changes into the signal $h(k)$ when the DC component is exponentially extended and the harmonic signal is sampled with the specified sampling time T_s.

$$h(k) = \sum_{n=1}^{Q} A_n \sin\left(\omega_n k T_s + \varphi_n\right) + A_0 \exp\left(-\alpha_0 k T_s\right) + n(k) \tag{6}$$

Subsequently, by applying a Taylor series expansion to the harmonic signal $h(t)$, the mathematical modeling of acceleration harmonic estimation is obtained. It is represented as follows:

$$h(k) = \sum_{n=1}^{Q} A_n \sin\left(\omega_n k T_s + \varphi_n\right) + A_0 - A_0 \alpha_0 k T_s + n(k) \tag{7}$$

The sine and cosine functions can be used to describe the harmonic signal $h(t)$, which can then be rewritten as follows:

$$\begin{aligned} h(k) = & \\ & \sum_{n=1}^{Q} [A_n \sin(\omega_n k T_s) \cos\varphi_n + A_n \cos(\omega_n k T_s) \sin\varphi_n] + \\ & A_0 - A_0 \alpha_0 k T_s + n(k) \end{aligned} \tag{8}$$

The mathematical modelling required to estimate sinusoidal acceleration harmonics is represented by the harmonic signal shown above. An extended acceleration harmonics prediction model can be derived by incorporating sub harmonics and intermediate harmonics into the aforementioned model, as expressed below.

$$\begin{aligned} h(k) = & (A_{\text{sub}} \sin(\omega_{\text{sub}} k T_s) \ldots \\ & \cos\varphi_{\text{sub}} + (A_{\text{sub}} \cos(\omega_{\text{sub}} k T_s) \sin\varphi_{\text{sub}} + \ldots \\ & \sum_{n=1}^{Q} [A_n \sin(\omega_n k T_s) \cos\varphi_n + A_n \cos(\omega_n k T_s) \sin\varphi_n] \ldots \\ & (A_{\text{int}} \sin(\omega_{\text{int}} k T_s) \cos\varphi_{\text{int}} + (A_{\text{int}} \cos(\omega_{\text{int}} k T_s) \ldots \\ & \sin\varphi_{\text{int}} + A_0 - A_0 \alpha_0 k T_s + n(k) \end{aligned} \tag{9}$$

where A_{sub} is the amplitude of the sub-harmonic, ω_{sub} is the frequency of the sub-harmonic and φ_{sub} is the phase of the sub-harmonic. Similarly, A_{int} is the amplitude of the inter-harmonic, ω_{int} is the frequency of the inter-harmonic and φ_{int} is the phase of the inter-harmonic.

Literature studies to date have primarily focused on the mathematical modelling of sinusoidal signals. In this study, the modelling is extended to sinusoidal, triangular, and square waveform signals, which is expected to provide novel experimental evidence and a broader dataset to the existing literature. The mathematical representations of the triangular and square waveforms are given in Eq. (10) and Eq. (11), respectively. This approach enables a more comprehensive analysis of the dynamic characteristics of different signal types, offering new insights for both

theoretical investigations and practical engineering applications. Future studies are anticipated to further expand the current literature by exploring the applicability of these waveform models across diverse engineering domains, thereby establishing a broader research framework.

Triangular wave model is expressed as follows [14]:

$$h(k) = \sum_{n=1}^{Q} A_n \text{sawtooth}\left(\omega_n k T_s + \varphi_n\right) + A_0 - A_0 \alpha_0 k T_s + n(k) \tag{10}$$

Square wave model is presented as follows [14]:

$$h(k) = \sum_{n=1}^{Q} A_n \text{square}\left(\omega_n k T_s + \varphi_n\right) + A_0 - A_0 \alpha_0 k T_s + n(k) \tag{11}$$

5 CO BASED ESTIMATION APPROACH

The CO algorithm is employed to estimate the amplitude and phase components of the sine, square, and triangular acceleration harmonic signals described above. The objective function presented below is used to guide the CO algorithm.

$$Objective = \min\left(\sum_{k=1}^{K} e^2(k)\right) = MSE\left(h_k - h_{k_{\text{estimated}}}\right) \tag{12}$$

where h_k is the simulated or experimental harmonic signal and $h_{k_{\text{estimated}}}$ is the harmonic signal estimated by the CO algorithm.

1. **Initialization:**
   1.1 Set population size N and maximum iteration number $MaxIter$.
   1.2 Randomly initialize the cheetah population W_i within the search bounds.
   1.3 Evaluate the objective function $f(W_i)$ for each cheetah.
2. **Objective Function Definition:**

$$f(W_i) = \frac{1}{n}\sum_{k=1}^{n}(h_k - \hat{h}_k(W_i))^2$$

where $\hat{h}_k(W_i)$ denotes the estimated harmonic signal using weight vector W_i.

3. **While (iteration < MaxIter) do**

(a) Cheetah's Search Phase:
– Explore the solution space randomly to locate potential prey regions.
– Update each cheetah's position:

$$W_i^{new} = W_i + r_1 \cdot (W_{rand} - W_i)$$

where r_1 is a random exploration coefficient.

(b) Cheetah's Waiting Phase:
– Reduce exploration and increase exploitation around promising areas.
– Update positions using:

$$W_i^{new} = W_i + r_2 \cdot (W_{best} - W_i)$$

where r_2 controls the trade-off between local and global search.

(c) Cheetah's Attack Phase:
– Intensify the search near the best solution (simulate prey attack behavior).
– Update W_i^{new} adaptively to minimize the objective function.

(d) Evaluate Objective Function:
– Compute $f(W_i^{new})$ for all cheetahs.
– Update W_{best} if a better solution is found.

4. **End While**
5. **Return** W_{best} as the optimal weight vector.
6. **Reconstruct** the harmonic signal using $\hat{h}(t; W_{best})$.

Figure 5 Pseudo code of proposed CO algorithm-based estimation approach

Fig. 5 presents the pseudocode of the proposed CO-based acceleration harmonic estimation method, while Fig. 6 illustrates its block diagram. To address the acceleration harmonic estimation problem, the fundamental control parameters of the CO algorithm are first established. Next, the experimental acceleration harmonic signal is input into the system. Using the mathematical models described in the previous section, the amplitude and phase values are estimated by processing the signal through the algorithmic steps of the CO algorithm. The mean square error between the acceleration harmonic signal generated with the estimated parameters and the experimental acceleration harmonic signal is used to guide the CO algorithm in optimizing the parameters. In the final stage, the optimal estimated amplitude and phase values are identified, errors are calculated, comparisons are made, and the program terminates.

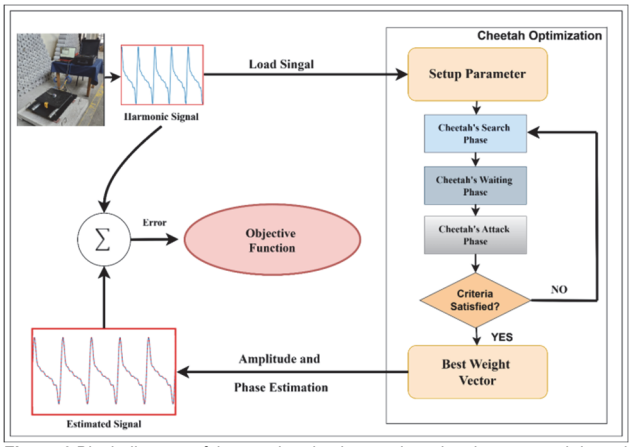

Figure 6 Block diagram of the acceleration harmonic estimation approach based on the CO algorithm

6 ANALYSIS AND RESULTS

To evaluate the performance of the CO-based acceleration harmonic estimation method on test and experimental harmonic signals, 30 runs were conducted using different seed values. The mean, standard deviation, best, and worst results were calculated across these runs. The control parameters of the CO algorithm were set as follows: a population size of 6, a group size of 2 search agents, and a maximum of 2000 iterations. The search space for the amplitude and phase parameters was defined broadly within the range [−20, 20]. This range was consistently applied to the estimated parameters for all test and experimental signals.

During shaking table experiments, displacement input data generated from frequency and displacement amplitude values are used as input signals. The responses resulting from these displacement inputs are measured by accelerometers mounted on the shaking table. Consequently, the data obtained from the shaking table are expressed in terms of acceleration. However, it is important to note that these acceleration data can also be processed to derive displacement data. In the experimental studies, the waveforms of the acceleration signals were varied among sine, square, and triangular shapes, and the input displacement amplitudes were selected as 3.5 mm, 5 mm, and 10 mm to analyse different conditions. Additionally, the CO-based acceleration harmonic estimation approach

was introduced to evaluate performance under these varying experimental conditions.

6.1 Analysis of the Test Signal

In the proposed harmonic estimation approach, a comparative analysis is conducted using a benchmark harmonic test signal to evaluate the convergence and error performance of the CO algorithm relative to metaheuristic algorithms presented in other studies. PSO, bat algorithm, ABC algorithm and MABC - ABC algorithm and CO algorithm were used for the competition. For CO algorithm, the comparison yielded the following results: the mean was 1.0032, the standard deviation was 3.2745, the best error value was $1.3669e^{-14}$, and the worst error value was 16.9130. With error rates of 0.0001% in the first harmonic degree, 0.0001% in the second, 0.0002% in the third, 0.0001% in the fourth, 0.0001% in the fifth, and 0.0004% in the sixth, the analysis's findings showed that superior results were achieved in all harmonic degrees compared to other competing algorithms. In the phase part, it outperformed the competing algorithms with an error rate of 0.0007% at the third-order harmonic. The CO algorithm outperformed the other competing algorithms in seven of the 12 parameters [13].

6.2 Analysis of Experimental Sinusaidal Signals

For the sinusoidal waveform, the experimental study was conducted using the shaking table both unloaded and with the load described in the previous section. In both conditions, various experimental scenarios were created by applying a frequency of 6 Hz and displacements of 3.55 mm., 5 mm., and 10 mm. to generate and capture the acceleration harmonic signals from the acceleration sensors. The CO-based acceleration harmonic estimation method was executed 30 times for each experimental scenario. Statistical values were calculated, and amplitude versus sample number and power spectrum versus frequency graphs were plotted for the best-predicted amplitude and phase values. For the 3.55 mm displacement under the loaded and unloaded operation case, Fig. 7 and Fig. 8 show the experimental acceleration harmonic signals and the signals estimated with the CO-based approach. Both figures include amplitude versus sample number and power spectrum versus frequency graphs. Therefore, the performance is evaluated through dual validation, utilizing both the time domain and the frequency domain. When analyzed in both the time and frequency domains, the experimental signal - under both loaded and unloaded conditions - closely matches the signal estimated using the proposed approach. It is important to note that six harmonics were estimated, and the estimation performance for these harmonics is quite accurate. Since no estimation was performed beyond the sixth harmonic, the resulting distortions are clearly visible. For the 5 mm. and 10 mm. displacements under both loaded and unloaded operating conditions, the experimental acceleration harmonic signals and those predicted using the CO-based approach are shown in Figs. 9, 10, 11, and 12. When the figures are examined for each case, the agreement between the experimental and predicted signals demonstrates that the prediction is both effective and robust.

Tab. 1. presents the mean, standard deviation, best, and worst values calculated from the statistical data obtained over 30 runs for each possible scenario. Tab. 2. displays the amplitude and phase values of the six harmonics estimated for the best error value. The results show that the load effect negatively impacts estimation performance at low amplitudes; however, as the amplitude increases, it significantly enhances harmonic estimation accuracy by improving the system's dynamic stability. According to Tab. 2., the CO algorithm accurately predicted the fundamental components of the sinusoidal signals. It was concluded that the system's nonlinear dynamic behavior became evident through an increase in the amplitudes of the second and third harmonic components, particularly under the influence of load.

Table 1 Mean, standard deviation (SD), best and worst error values of sinusoidal signals

Signal Type	Mean	SD	Best	Worst	Elapsed time / s
Without load (Displacement: 3.55 mm.)	0.4648	2.2219	0.0194	12.1745	0.892
Loaded (Displacement: 3.55 mm.)	0.9758	3.1470	0.1259	13.6363	0.883
Withoutload (Displacement: 5 mm.)	4.3643	14.1450	0.1406	70.8141	0.939
Loaded5 (Displacement: 5 mm.)	1.3730	3.8627	0.0932	15.1908	0.948
Withoutload (Displacement: 10 mm.)	6.4155	15.4191	0.8538	65.3702	0.932
Loaded (Displacement: 10 mm.)	1.6960	6.1229	0.2006	33.5603	0.926

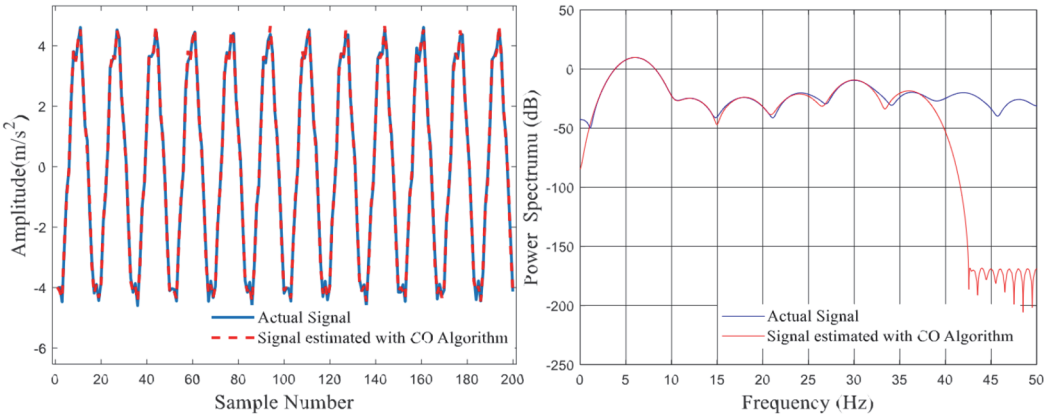

Figure 7 Amplitude vs. sample number (a) and power spectrum vs. frequency (b) of the unloaded sinusoidal signal (displacement: 3.55 mm) for actual signal and estimated signal by the CO algorithm

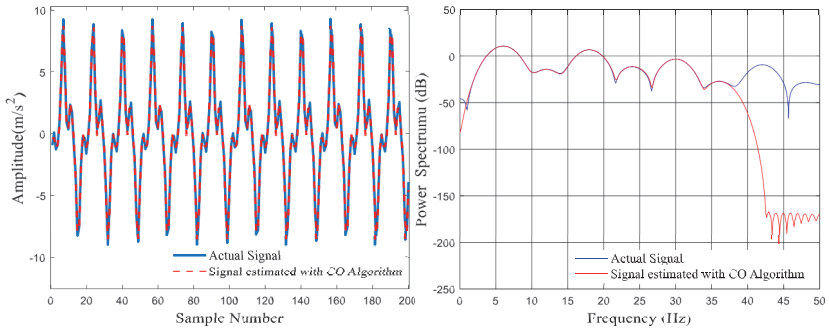

Figure 8 Amplitude vs. sample number (a) and power spectrum vs. frequency (b) of the loaded sinusoidal signal (displacement: 3.55 mm) for actual signal and estimated signal by the CO algorithm

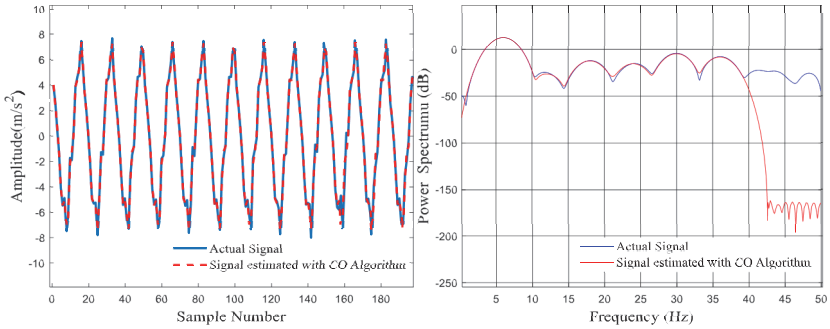

Figure 9 Amplitude vs. sample number (a) and power spectrum vs. frequency (b) of the unloaded sinusoidal signal (displacement: 5 mm) for actual signal and estimated signal by the CO algorithm

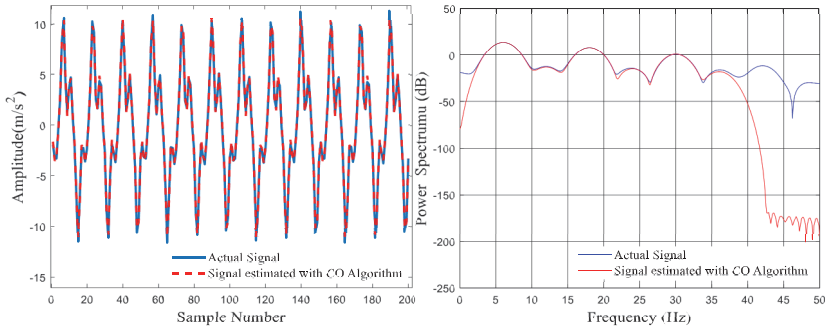

Figure 10 Amplitude vs. sample number (a) and power spectrum vs. frequency (b) of the loaded sinusoidal signal (displacement: 5 mm) for actual signal and estimated signal by the CO algorithm

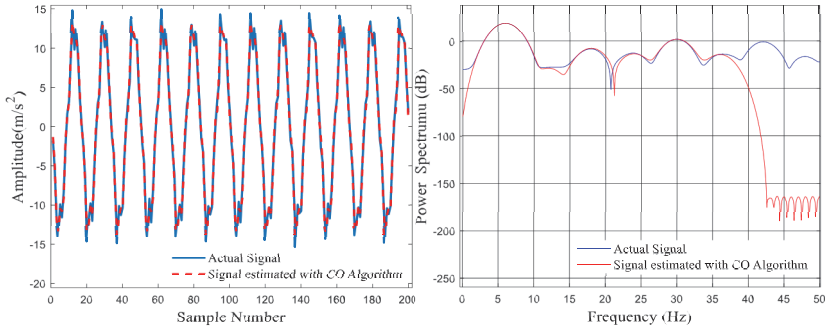

Figure 11 Amplitude vs. sample number (a) and power spectrum vs. frequency (b) of the unloaded sinusoidal signal (displacement: 10 mm) for actual signal and estimated signal by the CO algorithm

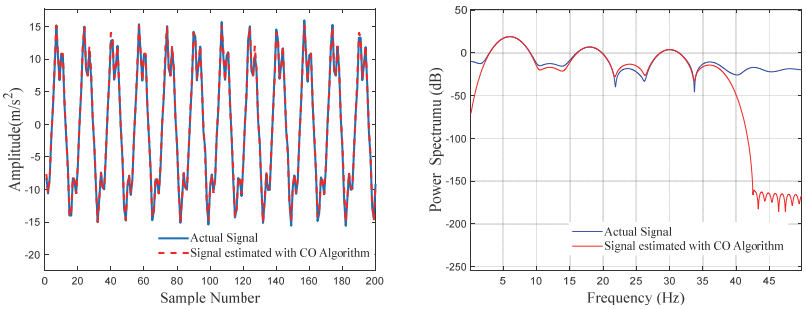

Figure 12 Amplitude vs. sample number (a) and power spectrum vs. frequency (b) of the loaded sinusoidal signal (displacement: 10 mm) for actual signal and estimated signal by the CO algorithm

Table 2 Estimated amplitude and phase values by CO algorithm for the best obtained error value of the sinusoidal signals

Signal Type	Parameters	Harmonics Degree					
		1.	2.	3.	4.	5.	6.
Without load (Displacement: 3.55 mm.)	Amplitude / m/s²	4.4193	0.0831	0.0918	0.1271	0.4934	0.1722
	Phase / radian	4.4825	−2.2212	−5.6219	−0.6352	7.6076	−6.7973
Loaded (Displacement: 3.55 mm.)	Amplitude / m/s²	4.8894	0.2698	3.0894	0.3832	0.9681	0.0620
	Phase / radian	5.4095	0.1533	−5.1105	−0.9000	−4.0653	−7.9307
Without load (Displacement: 5 mm.)	Amplitude / m/s²	6.2704	0.0733	0.3415	0.2426	0.8287	0.5591
	Phase / radian	−4.3746	−8.4202	1.9386	−2.8589	1.5333	−2.5979
Loaded (Displacement: 5 mm.)	Amplitude / m/s²	6.7132	0.3035	3.4673	0.2471	1.5051	0.1720
	Phase / radian	4.9987	5.8089	6.9632	4.6859	7.2894	−9.7833
Without load (Displacement: 10 mm)	Amplitude / m/s²	12.3789	0.0519	0.5791	0.2974	1.7517	0.2721
	Phase / radian	−0.1718	13.9049	−3.0628	6.7007	14.0962	8.1280
Loaded (Displacement: 10 mm.)	Amplitude / m/s²	12.6610	0.2026	3.1787	0.3094	2.2192	0.2749
	Phase / radian	−1.2101	6.9429	1.9516	−6.4994	−10.099	−6.9951

6.3 Analysis of Experimental Triangular Signals

Experimental studies on the triangular waveform were conducted using both unloaded and loaded shaking tables, applying a frequency of 6 Hz and displacements of 3.55 mm, 5 mm, and 10 mm. The CO-based acceleration harmonic estimation method was executed 30 times for each scenario, and statistical values were calculated. Amplitude versus sample number and power spectrum versus frequency graphs were plotted for the best predicted values.

The experimental and CO-based estimated acceleration signals in both the time and frequency domains for displacements of 3.55 mm, 5 mm, and 10 mm. under loaded and unloaded conditions are presented in Fig. 13 through 18. A comparative analysis of Fig. 13 through 18 reveals that external load significantly influences the characteristics of the vibration signal in both the time and frequency domains. Under no load, the actual signal and the signal predicted by the CO algorithm closely overlap in the time domain, demonstrating that the algorithm accurately captures both amplitude and phase components. Correspondingly, the fundamental frequency and its harmonics appear sharp and distinct in the power spectrum, and the predicted spectrum largely preserves this structure. In contrast, when the system is loaded, amplitude deviations and phase shifts become more pronounced in the time domain, reducing the agreement between the actual and predicted signals. The power spectrum under loaded conditions exhibits broader harmonic peaks, an elevated noise floor, and the emergence of additional spectral components, indicating nonlinear effects in the system and a reduced signal-to-noise ratio. Overall, the application of load disrupts the harmonic integrity of the signal and complicates the prediction process, resulting in decreased prediction accuracy of the CO algorithm compared to the unloaded condition.

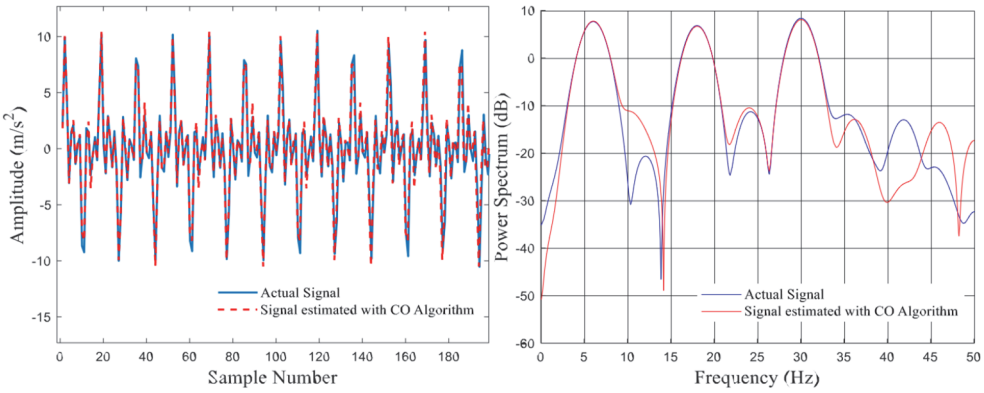

Figure 13 Amplitude vs. sample number (a) and power spectrum vs. frequency (b) of the unloaded triangle signal (displacement: 3.55 mm) for actual signal and estimated signal by the CO algorithm

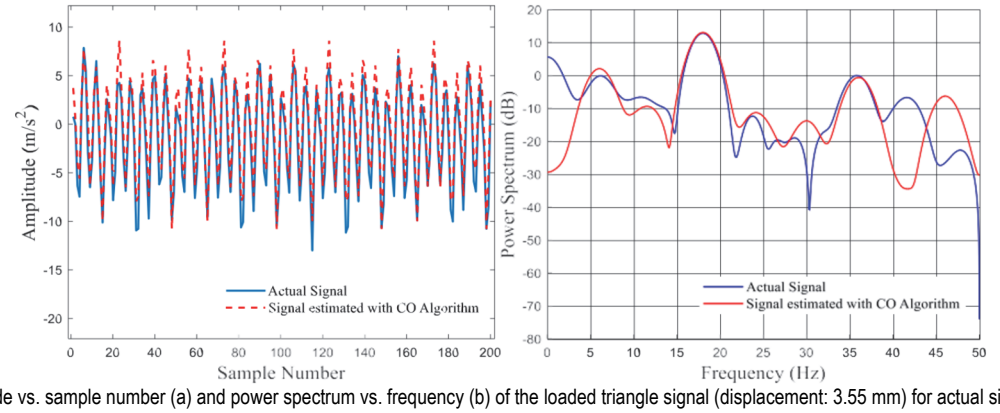

Figure 14 Amplitude vs. sample number (a) and power spectrum vs. frequency (b) of the loaded triangle signal (displacement: 3.55 mm) for actual signal and estimated signal by the CO algorithm

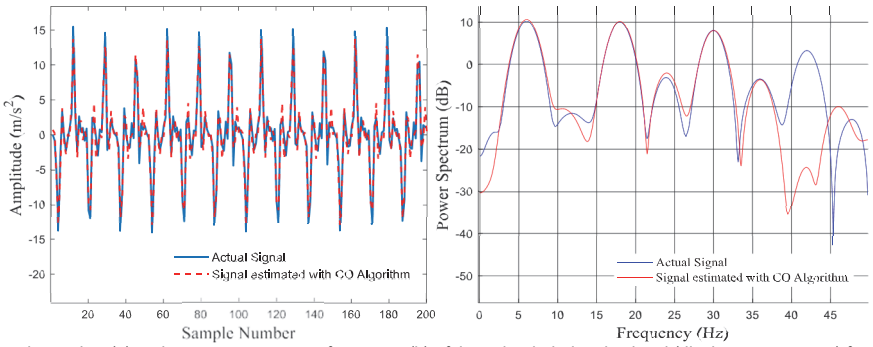

Figure 15 Amplitude vs. sample number (a) and power spectrum vs. frequency (b) of the unloaded triangle signal (displacement: 5 mm) for actual signal and estimated signal by the CO algorithm

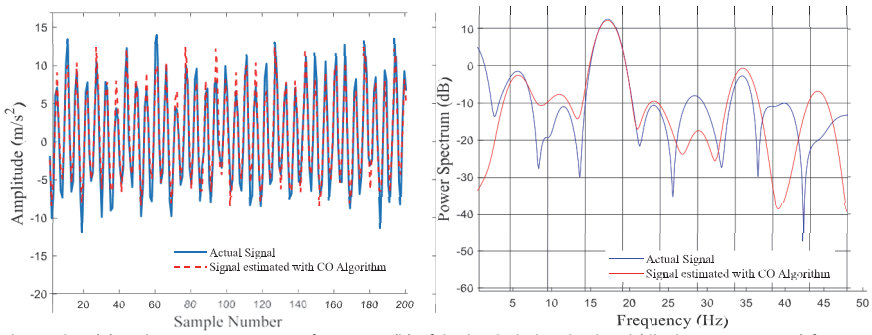

Figure 16 Amplitude vs. sample number (a) and power spectrum vs. frequency (b) of the loaded triangle signal (displacement: 5 mm) for actual signal and estimated signal by the CO algorithm

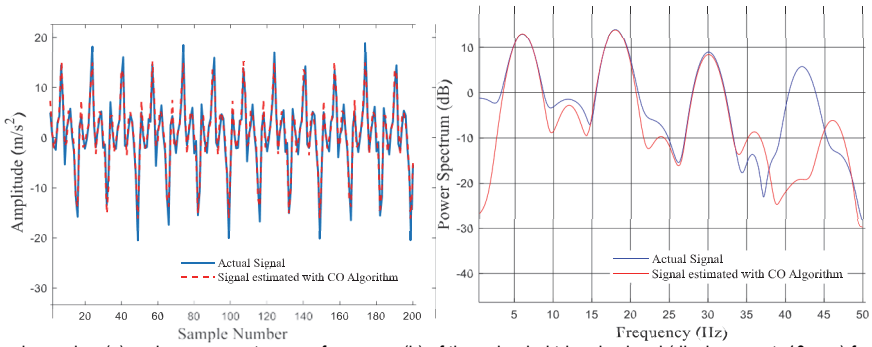

Figure 17 Amplitude vs. sample number (a) and power spectrum vs. frequency (b) of the unloaded triangle signal (displacement: 10 mm) for actual signal and estimated signal by the CO algorithm

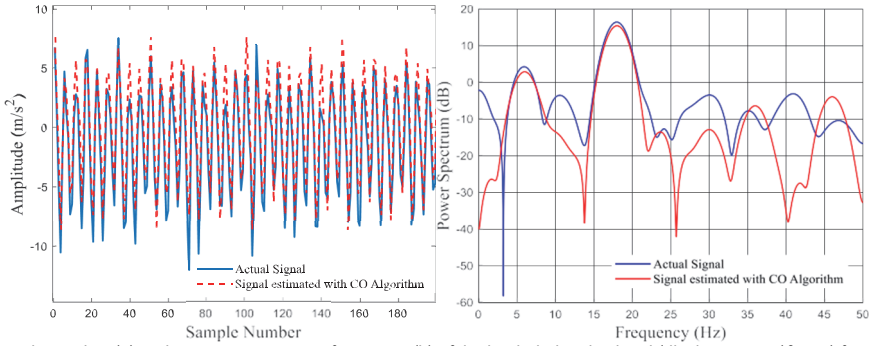

Figure 18 Amplitude vs. sample number (a) and power spectrum vs. frequency (b) of the loaded triangle signal (displacement: 10 mm) for actual signal and estimated signal by the CO algorithm

Tab. 3. presents the mean, standard deviation, best, and worst values calculated from the statistical data obtained over 30 runs for each scenario. The table indicates that the CO algorithm's performance depends on both loading and displacement. At 3.55 mm, it achieves low errors when unloaded, but loading significantly increases the error. At 5 mm, unloaded conditions result in high errors and instability, whereas applying a load improves consistency. At 10 mm, loading has little effect, with similar errors observed in both loaded and unloaded cases. Overall, the algorithm performs best at low displacements without load, while mid-level unloaded conditions lead to greater variability.

Tab. 4. displays the amplitude and phase values of the six harmonics estimated for the best error value. The CO algorithm accurately estimates the harmonic structure of triangular signals, but load and displacement variations significantly affect both amplitude and phase values.

Table 3 Mean, standard deviation, best and worst error values of the triangular signals

Signal Type	Mean	SD	Best	Worst	Elapsed time / s
Without load (Displacement: 3.55 mm.)	0.7813	2.4712	0.3087	13.8603	1.737
Loaded (Displacement: 3.55 mm.)	5.1956	6.1291	2.7205	26.9492	1.865
Without load (Displacement: 5 mm.)	8.1618	11.9736	2.3203	48.0504	1.871
Loaded5 (Displacement: 5 mm.)	3.2091	0.9118	2.8497	6.8906	1.860
Without load (Displacement: 10 mm.)	6.2568	5.6526	4.3987	30.8503	1.869
Loaded (Displacement: 10 mm.)	6.0794	5.6960	4.2099	23.5281	1.806

Table 4 Estimated amplitude and phase values by CO algorithm for the best obtained error value of the triangular signals

Signal Type	Parameters	Harmonics Degree					
		1.	2.	3.	4.	5.	6.
Without load (Displacement: 3.55 mm.)	Amplitude / m/s²	4.2902	0.1920	3.3942	0.5078	4.2768	0.4082
	Phase / radian	2.6034	5.0167	−4.1812	−2.7519	7.0511	6.5903
Loaded (Displacement: 3.55 mm.)	Amplitude / m/s²	2.1870	0.4939	7.7103	0.4217	0.3376	1.6456
	Phase / radian	−5.4426	0.7540	−9.1574	−2.5133	6.0121	−0.2617
Without load (Displacement: 5 mm.)	Amplitude / m/s²	5.8505	0.2669	4.9841	1.3736	4.1859	1.1798
	Phase / radian	5.1557	9.9274	3.4412	0.7780	−5.4906	−2.8090
Loaded (Displacement: 5 mm.)	Amplitude / m/s²	1.2639	0.5942	7.3566	0.5407	0.2579	1.5650
	Phase / radian	4.1232	−2.5133	3.0925	−4.5239	−8.6149	−1.0596
Without load (Displacement: 10mm)	Amplitude / m/s²	7.8148	1.2242	7.8609	0.5590	4.3182	0.6548
	Phase / radian	0.7469	1.5041	−9.7446	9.2662	3.4809	2.9667
Loaded (Displacement: 10 mm.)	Amplitude / m/s²	2.4481	0.1675	11.1310	0.4214	0.3319	0.8301
	Phase / radian	5.6303	8.1681	−1.2707	0.5027	3.1416	0.5931

6.4 Analysis of Experimental Square Signals

Experimental studies on the square waveform were conducted using both loaded and unloaded shaking tables at a frequency of 6 Hz and displacements of 3.55 mm, 5 mm, and 10 mm. The CO-based acceleration harmonic estimation method was run 30 times for each scenario, and statistical values were calculated. Amplitude-sample number and power spectrum-frequency plots were obtained for the best predicted values. The experimental and CO-based estimated acceleration signals for displacements of 3.55 mm, 5 mm, and 10 mm in both time and frequency domains are presented in Figs. 19 to 24.

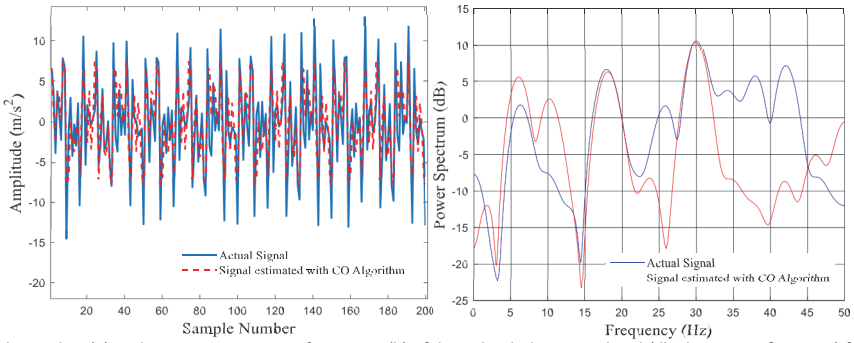

Figure 19 Amplitude vs. sample number (a) and power spectrum vs. frequency (b) of the unloaded square signal (displacement: 3.55 mm) for actual signal and estimated signal by the CO algorithm

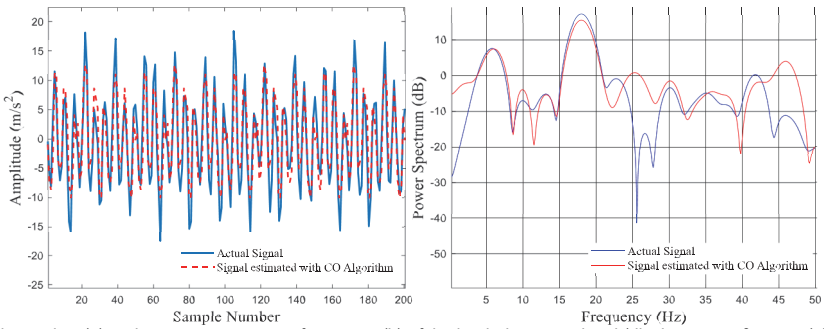

Figure 20 Amplitude vs. sample number (a) and power spectrum vs. frequency (b) of the loaded square signal (displacement: 3.55 mm) for actual signal and estimated signal by the CO algorithm

A comparative analysis of Figs. 19 to 24 shows that due to the structural characteristics of the square waveform, the CO algorithm has difficulty achieving the desired accuracy compared to sinusoidal and triangular waves, both under loaded and unloaded conditions. The abrupt transitions (sharp rising and falling edges) and high harmonic content of the square wave signal make it difficult to accurately capture both amplitude and phase components in the time domain. Therefore, even under unloaded conditions, significant differences emerge between the actual signal and the estimated signal. Furthermore, power spectrum analyses reveal that the square wave exhibits a broad-band spectral structure due to its high harmonic richness, and the CO algorithm struggles

to estimate these harmonic components with sufficient precision. Under loaded conditions, additional nonlinear effects and mechanical uncertainties arise in the system, leading to further deviations in both the time and frequency domains, and the estimated spectral structure fails to fully represent the actual signal. In general, the sharp transitions and high harmonic content inherent in the square waveform limit the harmonic estimation performance of the CO algorithm in both loaded and unloaded scenarios; the application of load further accentuates this complex structure, leading to a decrease in estimation accuracy.

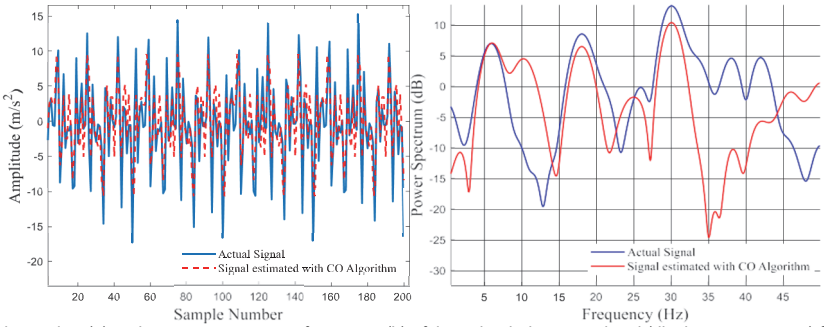

Figure 21 Amplitude vs. sample number (a) and power spectrum vs. frequency (b) of the unloaded square signal (displacement: 5 mm) for actual signal and estimated signal by the CO algorithm

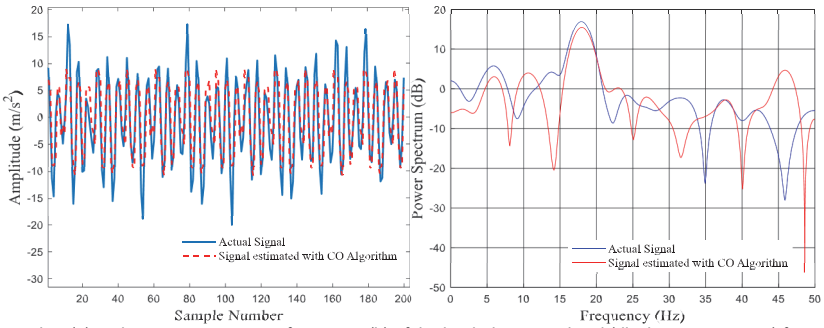

Figure 22 Amplitude vs. sample number (a) and power spectrum vs. frequency (b) of the loaded square signal (displacement: 5 mm) for actual signal and estimated signal by the CO algorithm

Table 5 Mean, standard deviation, best and worst error values of square marks

Signal Type	Mean	SD	Best	Worst	Elapsed time / s
Without load (Displacement: 3.55 mm.)	16.8594	10.5867	12.628	51.8302	1.771
Loaded (Displacement: 3.55 mm.)	19.5477	26.6753	12.916	159.582	1.861
Without load (Displacement: 5 mm.)	37.6488	67.6111	15.237	336.552	1.824
Loaded 5 (Displacement: 5 mm.)	24.4058	41.1512	14.843	237.386	1.957
Without load (Displacement: 10 mm.)	24.6156	20.8238	17.006	123.825	1.687
Loaded (Displacement: 10 mm.)	17.8150	30.5827	9.9737	177.691	2.174

Table 6 Estimated amplitude and phase values by CO algorithm for the best obtained error value of the square signals

Signal Type	Parameters	Harmonics Degree					
		1.	2.	3.	4.	5.	6.
Without load (Displacement: 3.55 mm.)	Amplitude / m/s²	2.0248	0.1868	1.5969	0.4312	3.2981	0.2995
	Phase / radian	−12.3633	11.9724	13.6217	−13.5960	14.1826	0.4607
Loaded (Displacement: 3.55 mm.)	Amplitude / m/s²	3.0059	0.5734	6.2624	0.6745	1.4056	0.7795
	Phase / radian	−13.4074	11.3984	2.7066	−6.0698	−7.0244	5.8816
Without load (Displacement: 5 mm.)	Amplitude / m/s²	2.2462	0.5988	2.9925	0.6724	3.7011	0.5306
	Phase / radian	5.2317	17.2709	18.4407	10.2164	−18.8656	4.4916
Loaded (Displacement: 5 mm.)	Amplitude / m/s²	2.0152	1.0014	6.3478	1.1881	0.7128	0.4409
	Phase / radian	−9.5947	6.9277	1.4506	−10.8186	−13.3753	−1.5933
Without load (Displacement: 10mm)	Amplitude / m/s²	4.5708	0.9998	5.3484	0.5201	2.9182	0.5728
	Phase / radian	4.6281	2.9707	−1.8925	19.3100	2.4291	13.2199
Loaded (Displacement: 10 mm.)	Amplitude / m/s²	1.8039	0.5383	4.9254	0.4815	1.4783	0.3613
	Phase / radian	18.2604	−1.7726	3.1390	−14.4484	10.5556	8.9745

Tab. 5 shows the mean, standard deviation, best, and worst error values obtained from 30 runs of each scenario for the square waveform. The results reveal that, unlike sinusoidal and triangular signals, the CO algorithm struggles to consistently represent the square wave structure under both loaded and unloaded conditions. At 3.55 mm displacement, high error values are observed regardless of load condition, indicating that the algorithm struggles to capture the sharp transitions of the square wave. At 5 mm, both loaded and unloaded conditions produce similarly unstable and erratic results, and increasing displacement does not seem to improve prediction accuracy.

Performance remains unchanged at 10 mm displacement, with high error values observed under both conditions. Overall, the CO algorithm fails to produce stable, low-error predictions for the square waveform; neither loading nor displacement changes significantly

improve performance. Tab. 6 shows the amplitude and phase values for the first six harmonics estimated under the lowest error condition. Due to the high harmonic content and abrupt transient characteristics of the square waveform, the CO algorithm produces significant deviations in both amplitude and phase estimates. Load and displacement variations further exacerbate these deviations, making it difficult for the algorithm to accurately reconstruct the harmonic structure of square wave signals. Tab. 5 presents the mean, standard deviation, best, and worst values calculated from the statistical data obtained over 30 runs for each scenario. Tab. 6 displays the amplitude and phase values of the six harmonics estimated for the best error value. The results show that the load effect negatively impacts estimation performance at low amplitudes; however, as the amplitude increases, it significantly enhances harmonic estimation accuracy by improving the system's dynamic stability. According to Tab. 6, the CO algorithm accurately predicted the fundamental components of the triangular signals. It was concluded that the system's nonlinear dynamic behavior became more apparent through the increase in the amplitudes of the second and third harmonic components, particularly under loaded conditions.

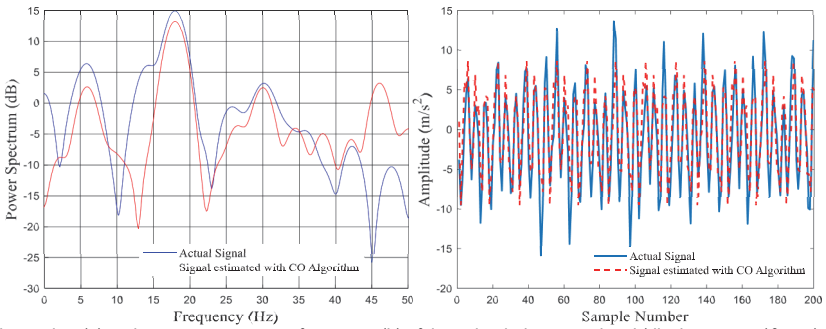

Figure 23 Amplitude vs. sample number (a) and power spectrum vs. frequency (b) of the unloaded square signal (displacement: 10 mm) for actual signal and estimated signal by the CO algorithm

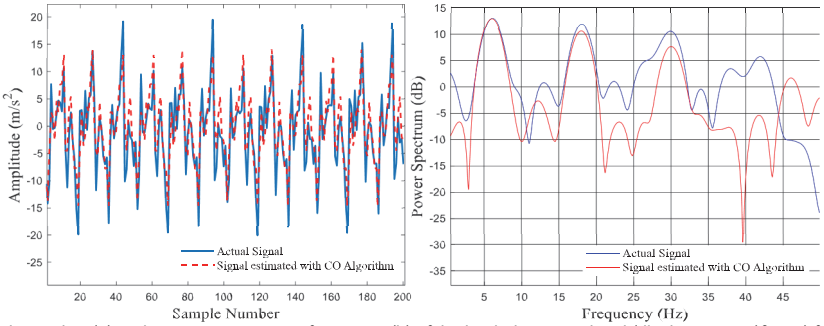

Figure 24 Amplitude vs. sample number (a) and power spectrum vs. frequency (b) of the loaded square signal (displacement: 10 mm) for actual signal and estimated signal by the CO algorithm

7 CONCLUSION

In this study, the performance of the CO algorithm in predicting harmonics in 18 different experimental acceleration signals (3 displacements, 3 waveforms, loaded/unloaded) obtained from a shaking table was investigated in detail. The findings demonstrated that the CO algorithm performed exceptionally well for sinusoidal signals. As seen in Tab. 1 and 2, the error rates remained low at all displacement levels, and the time and frequency domain plots (Figs. 7 to 12) showed that the predicted signal matched the true signal almost perfectly. In particular, an important observation was made that as the amplitude increased, the load increased the dynamic stability of the system, improving the prediction accuracy. In the analysis of triangular waveforms (Tabs. 3 and 4), it was found that the algorithm's performance varied depending on the load and displacement. The high agreement in the unloaded condition (Figs. 13, 15, 17) decreased when the load was added (Figs. 14, 16, 18). It was observed that load complicates the estimation process by disrupting the harmonic integrity of the signal. Square waveforms (Tabs. 5 and 6) were the most challenging scenario for the COalgorithm. Due to the sharp transitions in the waveform structure and the rich harmonic content, the algorithm failed to accurately capture the structure of the signal under both loaded and unloaded conditions, and high error values (Tab. 5) were observed in all scenarios. In conclusion, this study confirmed that the CO algorithm is a very effective and robust method for harmonic estimation of sinusoidal shaking signals. However, the algorithm's performance decreases as the signal complexity increases (triangular waves), and it cannot provide stable estimation for signals with sharp transitions such as square waves. These findings clearly indicate that future studies should focus on developing more advanced estimation models, particularly for these complex and nonlinear signal types.

Acknowledgment

I would like to thank Öğr. Gör. Dr. Fezayil SUNCA from Karadeniz Technical University for his support and assistance in obtaining real-time data and performing the shaking table experiment.

7 REFERENCES

[1] Bostenaru Dan, M. & Armas, I. (2015). Earthquake impact on settlements: The role of urban and structural morphology.

Natural Hazards and Earth System Sciences, *15*(10), 2283-2297. https://doi.org/10.5194/nhess-15-2283-2015

[2] Sun, L., Bai, Y., & Lai, Z. (2024). Shaking table test on seismic performance of a large-span high-rise building. *Scientific Reports*, *14*(1), 6580. https://doi.org/10.1038/s41598-024-57068-0

[3] Gao, C. H. & Yuan, X. B. (2019). Development of the shaking table and array system technology in China. *Advances in Civil Engineering*, *2019*, 8167684. https://doi.org/10.1155/2019/8167684

[4] Seki, K., Iwasaki, M., Kawafuku, M., Hirai, H., & Yasuda, K. (2008). Improvement of control performance in shaking-tables by feedback compensation for reaction force. *Proceedings of the 34th Annual Conference of the IEEE Industrial Electronics Society (IECON 2008)*, 2551-2556. https://doi.org/10.1109/IECON.2008.4758358

[5] Yao, J., Di, D., Jiang, G., Gao, S., & Yan, H. (2013). Real-time acceleration harmonics estimation for an electro-hydraulic servo shaking table using Kalman filter with a linear model. *IEEE Transactions on Control Systems Technology*, *22*(2), 794-800. https://doi.org/10.1109/TCST.2013.2256136

[6] Yao, J., Wan, Z., & Fu, Y. (2018). Acceleration harmonic estimation for hydraulic servo shaking table by using simulated annealing algorithm. *Applied Sciences*, *8*(4), 524. https://doi.org/10.3390/app8040524

[7] Yao, J., Yu, H., Dietz, M., Xiao, R., Chen, S., Wang, T., & Niu, Q. (2017). Acceleration harmonic estimation for a hydraulic shaking table by using particle swarm optimization. *Transactions of the Institute of Measurement and Control*, *39*(5), 738-747. https://doi.org/10.1177/0142331215619975

[8] Yao, J., Wan, Z., & Fu, Y. (2018). Acceleration harmonic estimation in a hydraulic shaking table using water cycle algorithm. *Shock and Vibration*, *2018*, 7278589.

[9] Kockanat, S. (2020). Acceleration harmonics estimation and elimination with MABC-RLS algorithm: Simulation and experimental analyses on shaking table. *Applied Soft Computing*, *92*, 106377. https://doi.org/10.1016/j.asoc.2020.106377

[10] Malathy, R. B., Bhat, G., & Dewangan, U. K. (2023). A hybrid algorithm for acceleration harmonic estimation and elimination in shake table. *Iranian Journal of Science and Technology, Transactions of Civil Engineering*, *47*(6), 3663-3680. https://doi.org/10.1007/s40996-023-01235-2

[11] Sunca, F. & Altunışık, A. C. (2022). Large-scale shake table tests on pounding response of RC buildings. *International Conference on Advanced Technologies for Humanity*, 49-60.

[12] Akbari, M. A., Zare, M., Azizipanah-Abarghooee, R., Mirjalili, S., & Deriche, M. (2022). The cheetah optimizer: A nature-inspired metaheuristic algorithm for large-scale optimization problems. *Scientific Reports*, *12*(1), 10953.

[13] Sunca, K. Y. & Koçkanat, S. (2024). Harmonic analysis of accelerometer signals using cheetah optimization algorithm. *Journal of Engineering Faculty*, *2*(2), 51-57.

[14] MathWorks. (2024). *Square and sawtooth function*. Signal Processing Toolbox.

Contact information:

Kadir Yasin SUNCA
(Corresponding author)
Sakarya University of Applied Sciences, Faculty of Technology,
54187, Sakarya, Turkey
E-mail: kadirsunca@subu.edu.tr

Serdar KOÇKANAT, Associate Professor
Sivas Cumhuriyet University, Faculty of Engineering,
58140, Sivas, Turkey
E-mail: skockanat@cumhuriyet.edu.tr